Three-dimensional band structure of graphite studied by angle-resolved photoemission using ultraviolet synchrotron radiation

D. Marchand, C. Frétigny, and M. Laguës
Laboratoire de Physique Quantique (Equipe de Recherche No. 676 associé au Centre National de la Recherche Scientifique), Ecole Supérieure de Physique et de Chimie Industrielles de la Ville de Paris, 10 rue Vauquelin, F-75231 Paris Cédex 05, France

F. Batallan, Ch. Simon, and I. Rosenman
Groupe de Physique des Solides de l'Ecole Normale Supérieure (Laboratoire No. 17 associé au Centre National de la Recherche Scientifique), Université de Paris VII, 2 place Jussieu, F-75251 Paris Cédex 05, France

R. Pinchaux
Laboratoire pour l'Utilisation du Rayonnement Electromagnétique, Université de Paris—Sud, Bâtiment 209C, F-91405 Orsay, France
(Received 6 April 1984)

Angle-resolved photoemission using synchrotron radiation from single crystals of natural graphite is reported for the first time. Direct as well as indirect transitions are observed. The π bands and the top of the σ bands are obtained with the assumption of a two-dimensional dispersion. A détailed discussion of the three-dimensional dispersion is presented for the π bands. In the Δ direction, the normal dispersion is described and leads to an effective mass of $m_{\perp}^{*}=1.2m$. Near the line P, the π bands are analyzed with use of the Slonczewski-Weiss-McClure model. Numerical values for the parameters within this model are derived. Some general features of the conduction bands at low energy are also given. Finally the experimental results are compared with the band-structure calculations.

I. INTRODUCTION

Graphite is a layered semimetal made of stacked carbon-atom planes. In addition, graphite forms intercalation compounds and serves as a substrate for physisorbed systems. There are at present numerous published works about its electronic properties. It is currently accepted that the band structure of graphite is formed as the energy is increased, by σ-bonding bands, π-bonding bands, π^{*}-antibonding bands, and σ^{*}-antibonding bands. The Fermi level (E_F) lies between the bonding π and antibonding π^{*} bands.

The works about the electronic structure of graphite may be classified in two categories. The first one concerns a particular aspect of the electronic structure. For example, the optical transitions are well explained by Painter and Ellis[1] within a two-dimensional (2D) band-structure model. The anisotropy of the Fermi-surface ellipsoidal pockets, which is about 16,[2] may be explained by a three-dimensional phenomenological approach of the π bands: the Slonczewski-Weiss-McClure[3] model. The second category of studies are experiments of which the results disperse on the whole electronic structure of graphite, e.g., x-ray form factor,[4] Compton effect,[5] or photoemission spectroscopy.[6–10] There are several studies of photoemission spectroscopy, which use either fully integrated[7] or angle-resolved photoemission;[6,8–10] taking as a light source either a helium lamp[6,9,10] or synchrotron radiation[7,8] with highly oriented pyrolytic graphite[6,8,9] or single-crystal samples[7,10]. These studies are mainly limited to a 2D analysis of the band structure.

We present here data obtained on single-crystalline graphite by ultraviolet angle-resolved photoemission spectroscopy (ARPES) using synchrotron radiation with variable photon energy. We have observed direct and indirect transitions associated unambiguously with initial and final states. The valence band for binding energies between about 10 eV and the Fermi level was obtained. We also observed a three-dimensional dispersion mainly for the π bands which are studied very carefully in the $\Gamma-A$ (Δ) and near the $K-L$ (P) directions. The analysis of this dispersion allows us to show the 3D structure of the valence band. Finally we compare our results with the band-structure calculations.

II. ANGLE-RESOLVED PHOTOEMISSION

A. Principles

In a photoemission experiment the electrons in a solid are excited by a monochromatic radiation $\hbar\omega$. Some electrons, after transport to the surface, have enough energy to pass across the surface potential barrier and to escape into the vacuum. In ARPES we detect in a well-defined geometrical direction the kinetic energy $E_k(k^{\text{ext}})$ of the electron in the vacuum.[11]

As the momentum component of the photoelectron $k_{||}$ parallel to the surface is conserved during the escape of the electron through the surface, it is given by

$$\hbar k_{||}=(2mE_k)^{-1/2}\sin\theta\ , \tag{1}$$

where θ is the polar angle of emission. E_k and $k_{||}$ are simultaneously measured for each photoelectron. The kinetic energy E_k of the photoelectron is referred to as the vacuum level. The final energy of the photoelectron E_f in the crystal, referred to as the Fermi level, is given by

$$E_f(k)=E_k(k^{\text{ext}})+W\ , \tag{2}$$

where W is the work function.

There are several processes which lead to an excited state.

(i) Direct transitions of an electron from the valence-band to the conduction band with conservation of $\vec{k}$. These processes obey the relation

$$E_i(k)=E_f(k)-\hbar\omega\ , \tag{3}$$

where E_i is the initial energy of the electron.

From direct transitions we obtain $E_i(k_{||})$, which describes the valence band, and $E_f(k_{||})$, the conduction band. However, the resolution of the conduction band is highly limited by the lifetime of electrons in their levels.

(ii) Indirect transitions with conservation of energy. These processes usually give the initial energy E_i of states with a high density in the valence band.

(iii) Indirect transitions without conservation of energy. From these processes we obtain $E_f(k_{||})$ for some levels, usually of high density of states in the conduction band.

Peaks which correspond to the three categories of transitions were observed. However, we are mainly interested in direct transitions which describe the bands. Therefore, we must first identify the nature of the peaks in order to separate direct and indirect transitions. By using synchrotron radiation, an almost unambiguous identification is possible. We study the evolution of the spectra as a function of the photon energy and the detector angle and finally, we use the existing band calculations as guides. Given that the $k_\perp$ component is not measured in ARPES, some supplementary assumptions are necessary in order to obtain the whole band structure.

B. Experimental setup

Angle-resolved photoemission experiments were performed using the synchrotron radiation of the Orsay storage-ring facilities, [Laboratoire pour l'Utilisation du Rayonnement Electromagnétique émis par les Anneaux de Collisions de l'Accélérateur linéaire d'Orsay (LURE-ACO)]. The light flux was monochromatized by a grazing-incidence monochromator. The angle-resolving photoelectron spectrometer provides an angular resolution of $\pm 0.5°$ and a total energy resolution of 200 meV. The photon-incidence angle, measured from the surface normal, was kept constant at 45° (s-p polarization).

The samples, natural graphite single crystals, are mounted and cleaved in a preparative ultrahigh-vacuum system ($\sim 10^{-9}$ mbar). The samples were then transferred into the experimental chamber[12] (10^{-11}-mbar range). The resulting fresh basal-plane surfaces were analyzed and oriented by means of low-energy electron diffraction. The diffraction pattern preserved its sharpness for at least three days under ultrahigh-vacuum conditions. No changes were observed in the angle-resolved uv photoemission spectra during this time either, confirming that the surface remained free of contaminants.

The electron-energy analyzer is rotated in the incidence plane to vary the polar angle θ of photoemission from the sample. The azimuthal angle φ is kept constant at 0° and 30°, which correspond, respectively, to the ΓALM ($U\Delta$) and ΓAHK ($P\Delta$) planes in the Brillouin zone (BZ).

III. RESULTS

We have studied several samples for the two main planes of the Brillouin zone, $P\Delta$ and $U\Delta$, as a function of both the photon energy and the detector angle. A considerable amount of data was obtained for photon energies between 14 and 28 eV. Figure 1 presents two typical scans in the $U\Delta$ and $P\Delta$ planes for various detection angles θ with incident photon energies of 21.2 and 24 eV, respectively. Given that the graphite is a layered material, the first approach to its electronic structure is to neglect the dispersion along the c axis. This assumption is the two-dimensional approach.

A. Two-dimensional approach

The standard analysis of E_i as a function of $k_{||}$ for various photon energies [Eqs. (1) and (3)] was performed in order to obtain the valence band from direct transitions. The results are complicated by the presence of indirect transitions in the experimental spectra. Figure 2 presents E_i as a function of $k_{||}$ for the direct and indirect transitions in which the energy is conserved. In the $U\Delta$ plane the photon energy used is 21.2 eV, and in the $P\Delta$ plane, 24 eV. However, in this plane, we cannot obtain the whole π band with only one photon energy because some transitions are not allowed by the final-states structure. We thus plot supplementary points for $\hbar\omega=19$ eV. As a guide for eyes we have superimposed on the experimental points the shaded region corresponding to the π bands and the top of the σ bands as predicted by band calculations (Sec. IV) and fitted to our experimental results.

In Fig. 3 (for comparison with Fig. 2) we have represented the initial energy as a function of $k_{||}$ for photon energies between 14 and 28 eV. We observed the direct transitions as well as indirect transitions with conservation of energy. These results show a dispersion of the bands for different photon energies. This means that the three-dimensional effects are important, mainly for the π bands, and that it is necessary to analyze them as a function of $k_\perp$. A strong sharp peak located at $E_f=7.6$ eV, independent of the photon energy, was also observed which corresponds to indirect transitions without conservation of energy. This state has been observed up to about $k_{||}\sim 1$ Å^{-1} in the $U\Delta$ plane, and only near the Δ line in the $P\Delta$ plane. We will study the three-dimensional effects in two cases: The normal emission ($k_{||}=0$) and the constant $k_{||}$ emission near the line P (boundary zone).

B. Normal emission and three-dimensional effects

We have studied the normal emission for photon energies between 15 and 28 eV. Figure 4 shows a set of normal-emission spectra for different photon energies as a function of the initial energy. The sharp peak located at

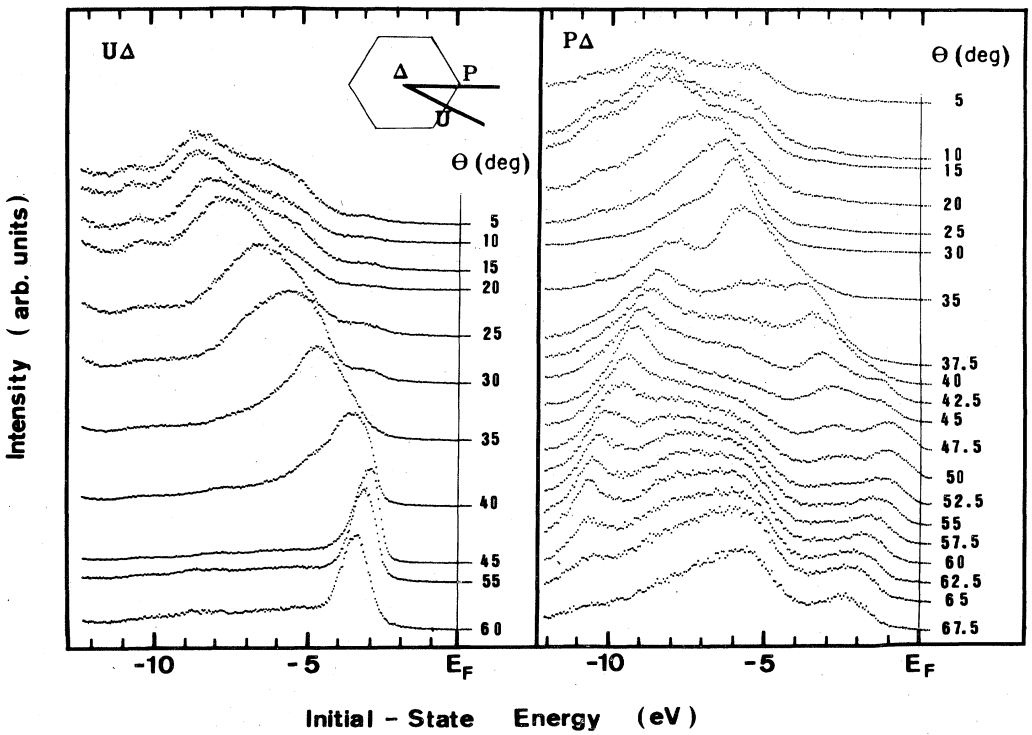

FIG. 1. Energy-distribution curves for different values of the polar angle θ. The photon energy $\hbar\omega$ is 21.2 eV in the $U\Delta$ plane and 24 eV in the $P\Delta$ plane. The main features correspond to the σ and π valence bands which superimpose for $\theta \sim 30°$. The zone boundary is attained in both cases for $\theta \sim 50°$.

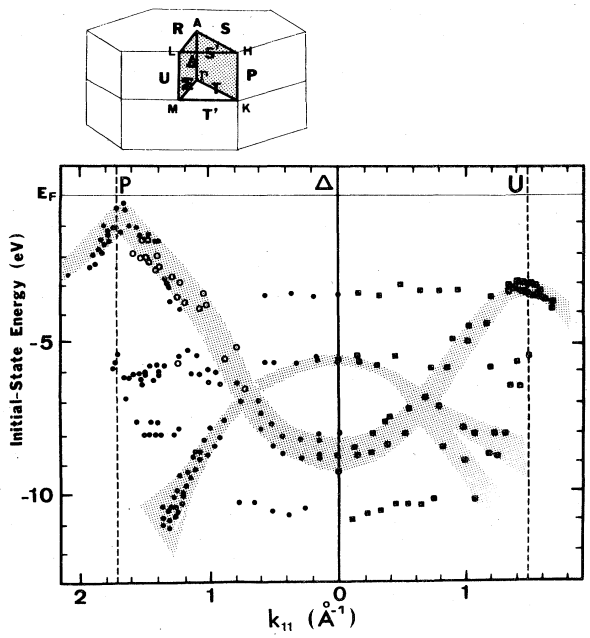

FIG. 2. Initial-state energy of the peaks versus $k_{||}$ for $\hbar\omega = 21.2$ eV (■) in $U\Delta$ plane and for $\hbar\omega = 19$ (○) and 24 eV (●) in $P\Delta$ plane. The choice of these last two energies shows the importance of the effect of final states, for instance, in the range $E_i > -5$ eV. The shaded area presents the generally accepted shape of π and σ bands, fitted to our experimental results. The Brillouin zone of graphite is shown in the upper part of the figure.

$E_f = 7.6$ eV independent of the photon energy (marked by an arrow) corresponds to indirect transitions without conservation of energy. We also observed the $k_\perp$ dispersion of peaks associated with direct transitions with dramatic effects of their cross sections. From their study we can describe the valence and conduction bands along the Δ direction.

Figure 5 presents the initial-state energy E_i as a func-

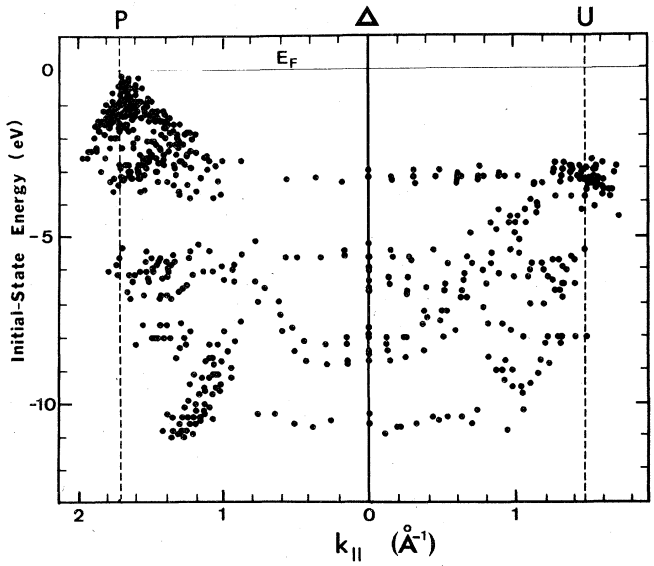

FIG. 3. Initial-state energy versus $K_{||}$ for all observed peaks (about 800), $\hbar\omega$ varying from 14 to 28 eV.

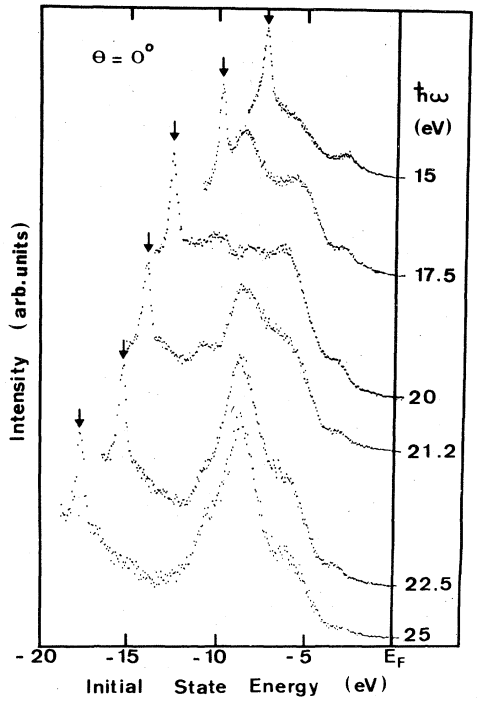

FIG. 4. Energy-distribution curves versus initial-state energy at normal emission ($\theta=0$), for several photon energies. The sharp peak marked by an arrow corresponds to a final state $E_f=7.6$ eV. The evolution of the shape and intensity of the other peaks reflects the $k_\perp$ dispersion of the valence band and the importance of the final states. For $\hbar\omega=17.5$, 22.5, and 25 eV, the π bands are nearly degenerated in a sharp peak at $E_i=-8.3$ eV.

tion of the final-state energy E_f for normal emission. For the sake of clarity, the E_i energies are limited to the range -4 to -10 eV. Indirect transitions (not presented in Fig. 5) were observed; they are associated with strong density-of-states features. In Fig. 5, features corresponding to the top of the σ bands and bottom of the π bands are visible. The top of the σ bands is found at -5.3 ± 0.1 eV with a small $k_\perp$ dispersion. The bottom of the π bands is centered at -8.3 eV and has a strong $k_\perp$ dispersion: 1.4 eV.

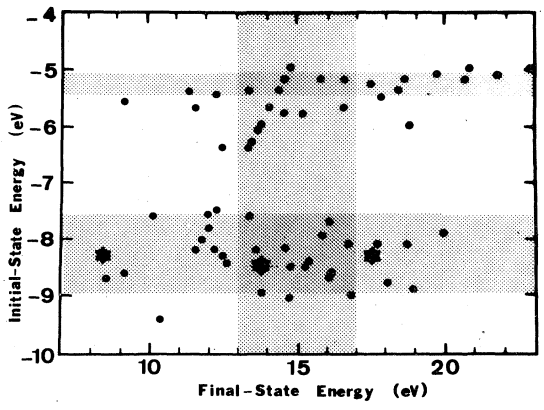

FIG. 5. Plot of E_i versus E_f at the normal for several photon energies. The shaded strip centered at $E_i=-5.3$ eV corresponds to the σ band with a small width (0.3 eV) of the order of the experimental resolution. The shaded strip centered at $E_i=-8.3$ eV corresponds to the π bands with a width of 1.4 eV due to the $k_\perp$ dispersion. The shaded strip at $E_f=15\pm2$ eV is a range of high-intensity peaks due to a final state. The three asterisks corresponds to direct transitions originating from the degenerated π bands near the A point.

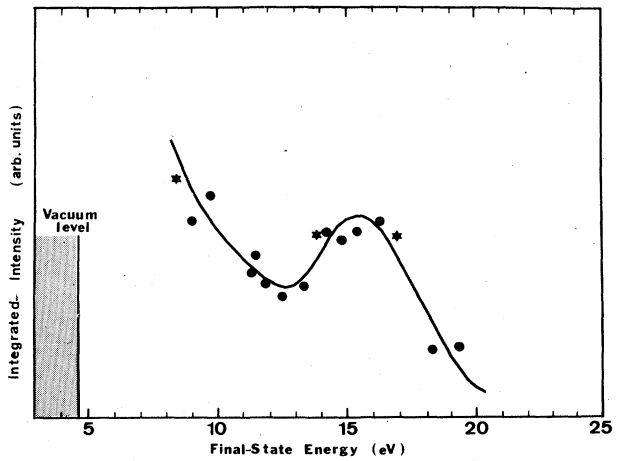

FIG. 6. Integrated intensity at $\theta=0$ of the direct transitions originating from the π bands versus the final-state energy for photon energies $\hbar\omega$ between 15 and 28 eV. The areas are normalized to the area of the sharp peak at $E_f=7.6$ eV. The three stars correspond to the degenerated π bands near the A point.

For direct transitions originating from the π bands as initial state we have calculated the integrated intensity of the photoemission peaks which is reported in Fig. 6 as a function of the final energy. The integrated intensity is proportional to the density of final states along the line Δ.[13] We observe a high density of states around $E_f=15$ eV. The 4-eV width is due to both the band structure in this energy range and the electron lifetime in the conduction band. It is known from symmetry considerations that the π bands merge in a twice-degenerated band at the A point. We attribute three peaks (Fig. 4 and 6) to direct transitions near the A point. These three very narrow peaks have the same initial energy $E_i=-8.3\pm0.1$ eV and are situated at the middle of the π band dispersion. The direct transitions at the Γ point correspond to either border of the π dispersion. We can describe the dispersion of the two π bands along the Δ direction by the relations

$$E_1(k_\perp)=E_1^0+\hbar^2k_\perp^2/2m_\perp^* ,$$

$$E_2(k_\perp)=E_2^0-\hbar^2k_\perp^2/2m_\perp^* ,$$

where $E_1^0=-9.0$ eV, $E_2^0=-7.6$ eV, and the effective mass $m_\perp^*=1.2m_0$.

Table I summarizes the numerical values obtained for the high-symmetry directions. From our results we obtain very accurate determinations because we observe indirect transitions with energy conservation associated with the strong density of states of these high-symmetry directions.

TABLE I. Experimental values of the energy position (eV) of the π, σ, and σ^* bands at the high-symmetry points of the Brillouin zone.

Band \ Point	Γ	M	K	A	L
π	-9.0 ± 0.1	-3.0 ± 0.1	-1.05 ± 0.1	-8.3 ± 0.1	-2.7 ± 0.1
π	-7.6 ± 0.1	-2.4 ± 0.1	-0.35 ± 0.1		
σ	-5.3 ± 0.1	-8.8 ± 0.3	-10.5 ± 0.2		
σ^*	$+7.6\pm0.1$				

C. Three-dimensional effects near the line *P*

The Fermi level cuts the π bands near the line *P*. The band structure has been extensively studied at this energy with Fermi-surface techniques.[2] We have devoted a large set of measurements to the study of the *P* direction and the surrounding range in the $P\Delta$ plane. For $k_{\parallel} \geq 1$ Å^{-1} in this plane, about ten different photon energies were used, whereas only two were used for lower $k_{\parallel}$. Figure 7 shows the initial-state energy of the main peaks as a function of $k_{\parallel}$ in the $P\Delta$ plane near the line *P*.

The well-known Slonczewski-Weiss-McClure model of (SWMcC) describes the π bands near the line *P*.[3] This model, which was extensively used for the Fermi-surface studies, uses seven phenomenological parameters: Δ, $\gamma_0, \ldots, \gamma_5$. For the $P\Delta$ and *UP* planes, the energy of the two π bonding bands is given by the following analytical expressions:

$$Ev_1 = \tfrac{1}{2}[\Delta + (\gamma_1 + \gamma_3\sigma)\Gamma + \tfrac{1}{2}(\gamma_2+\gamma_5)\Gamma^2] - \tfrac{1}{2}\{[\Delta + (\gamma_1 - \gamma_3\sigma)\Gamma + \tfrac{1}{2}(-\gamma_2+\gamma_5)\Gamma^2]^2 + 4(-\gamma_0+\gamma_4\Gamma)^2\sigma^2\}^{1/2}, \quad (4)$$

$$Ev_2 = \tfrac{1}{2}[\Delta - (\gamma_1 + \gamma_3\sigma)\Gamma + \tfrac{1}{2}(\gamma_2+\gamma_5)\Gamma^2] - \tfrac{1}{2}\{[\Delta - (\gamma_1 - \gamma_3\sigma)\Gamma + \tfrac{1}{2}(-\gamma_2+\gamma_5)\Gamma^2]^2 + 4(\gamma_0+\gamma_4\Gamma)^2\sigma^2\}^{1/2}, \quad (5)$$

with

$$\Gamma = 2\cos(k_{\perp}c),$$

$$\sigma = (\sqrt{3}/2)ax,$$

where a and c are the lattice constants of graphite and x the in-plane wave vector measured from the line *P*.

Among the seven parameters of the SWMcC model, our results are only sensitive to four of them: γ_0, γ_1, γ_3, and γ_4. For the other parameters, which are 1 order of magnitude smaller, we take their usual values[14] and adjust the former ones. The parameter γ_0 is related to the mean slope versus σ and γ_1 to the width of the band on the line *P*. The parameters γ_3 and γ_4 determine the differences between the slopes of both bands in the first and second B.Z. In Fig. 7 the experimental results are superimposed to the SWMcC dispersion relation of the π valence bands calculated in the Γ–*K* and *A*–*L* directions. The best agreement is found for $\gamma_0 = 3.3\pm0.15$ eV, $\gamma_1 = 0.4\pm0.05$ eV, $\gamma_3 = 0.33\pm0.10$ eV, and $\gamma_4 = -0.01\pm0.05$ eV. These values are also in good agreement with the values determined by other experiments.[14]

The origin of the bands calculated through the SWMcC model is shifted by 0.025 Å^{-1} towards Γ and by 0.350 eV towards negative energies. The shift of momentum is probably due to a polar angle θ misalignment of the order of 1°. If the energy shift is due to an azimuthal misalignment, the value should be about 5°. However, numerical calculations for $\phi = 5°$ with the SWMcC model are in

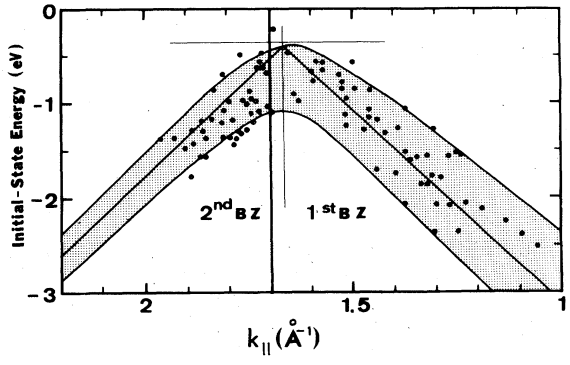

FIG. 7. The initial-state energy of the main peaks observed in the $P\Delta$ plane around the *P* direction versus $k_{\parallel}$. The SWMcC model is superimposed in bold lines for the ΓMK plane (upper and lower curves) and the *ALH* plane (middle curve). The shaded area corresponds to the π band dispersion between these limits. The SWMcC parameters are chosen in agreement with our results. The calculated bands are shifted by 0.025 Å^{-1} towards Γ and by 0.35 eV towards negative energies.

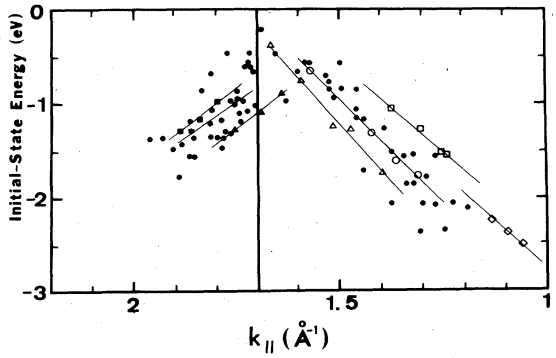

FIG. 8. The initial-state energy of the main peaks observed around the *P* direction versus $k_{\parallel}$. Peaks arising at a constant final-state energy within a width of ±0.25 eV are selected: $E_f = 11.75$ eV (◇), $E_f = 12.75$ eV (□), $E_f = 15.25$ eV (○), $E_f = 17.25$ eV (△), $E_f = 18.75$ eV (▲), $E_f = 20.75$ eV (*), $E_f = 23.75$ eV (■).

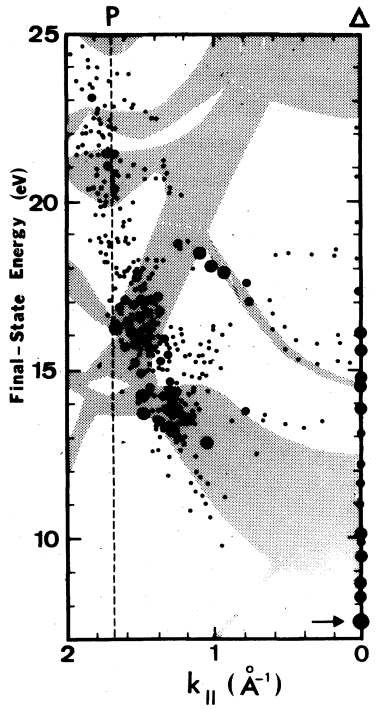

FIG. 9. Final-state energy corresponding to the peaks observed in the $P\Delta$ plane versus $k_{\|}$. The main peaks are figured by larger points. The shaded area is a two-dimensional projection of the bands calculated by Tatar and Rabii shifted by 1 eV towards higher E_f.

complete disagreement with the experimental points. The energy shift then has a physical meaning and corresponds to an excess of about 10^{-3} electron charge by the carbon atom. Since our results are only sensitive to the first layers, any surface defects or slight contamination could be sufficient to shift the bands by 0.350 eV. On the other hand, the energy reference in the surface layer may be shifted relative to the bulk level because of the presence of surface states.[15] In Fig. 8, seven sets of points are presented which correspond to a fixed final energy E_f. In these cases, the observed dispersion seems to be mainly the $k_{\|}$ dispersion of the initial state, in good agreement with the SWMcC description.

Figure 9 presents the final-state energy as a function of $k_{\|}$ for direct transitions in the $P\Delta$ plane. The sharp indirect transition at $E_f=7.6$ eV is also presented and marked by an arrow. The features around $E_f=15.7$ and 18.7 eV correspond, respectively, to the π and σ valence bands for $\hbar\omega=24$ eV. The shaded area is a two-dimensional projection of the band calculation made by Tatar and Rabii,[16] shifted by 1 eV to higher energies.

IV. DISCUSSION

Many band-structure calculations of graphite are now available. In order to interpret our photoemission results we have used three of them which are well adapted for the photoemission studies.

Willis *et al.*[17] have made a band-structure calculation extending over a 80-eV energy range in order to interpret their secondary electron-emission spectroscopy results. They used a linear variational approach taking Bloch basis as trial function. Their Hamiltonian takes into account the effective Coulomb potential and the exchange-correlation terms. They calculate the bands only in the basal plane because the dispersion along $k_{\perp}$ is smaller than the computed accuracy. This 2D model is very popular and has been used for analysis of the first photoemission studies in graphite.

Tatar and Rabii[16] calculated the electronic structure of three-dimensional graphite using a modified version of the Korringa-Kohn-Rostoker (KKR) technique. In the first step a KKR calculation is performed on a muffin-tin form of the crystal potential. This step is followed by diagonalizing the non-muffin-tin Hamiltonian in the muffin-tin basis.

Holzwarth *et al.*[18] have made a first-principles self-consistent calculation using the density-functional theory in the local-density approximation, and mixed-basis pseudopotential techniques.

The numerical values found in these three calculations for high-symmetry points are given in Table II. The valence band and the conduction band will now be discussed.

A. The valence band

The general characteristics of the valence band are now well established: It is formed by the σ- and π-bonding bands. As the energy increases one finds successively at the Γ point the bottom of the σ bands, the bottom of the π bands, and the top of the σ bands. The top of the π bands is at the Fermi level near the line P. Moreover, contrary to the σ bands, the π bands present a $k_{\perp}$ dispersion.

Our experimental results are in agreement with these features. The bottom of the π bands is located on the Δ line. In this direction the experimental width is 1.4 ± 0.2 eV. Their two extreme values correspond to the Γ point where we have two π bands located at -9.0 ± 0.2 eV and -7.6 ± 0.2 eV. These two bands are degenerated at -8.3 ± 0.2 eV at the A point. We describe the π dispersion along Δ as a parabolic band characterized by the effective mass $m_{\perp}^{*}=1.2m_0$. Near the line P in the $P\Delta$ plane our results are in good agreement with the SWMcC description, using the following set of parameters: $\gamma_0=3.3\pm0.15$ eV, $\gamma_1=0.4\pm0.05$ eV, $\gamma_3=0.33\pm0.1$ eV, and $\gamma_4=-0.01\pm0.05$ eV, which are close to the currently used values.[14]

The widths of the π bands are in agreement with the estimation of the band calculations. The position of the π bands agrees best with calculations of Holzwarth *et al.*[18] (Tables I and II).

The top of the σ band is also located on the line Δ at -5.3 ± 0.1 eV. Within the experimental error there are no dispersions, along the Δ direction. This value is lower than the estimations of the band calculations. In the line U, we find that the π bands are located at 2.4 and 3.0 eV at the M point, and merge at 2.7 eV at the L point.

TABLE II. Comparison between different calculations of the energy position (eV) for the π, σ valence bands and the lowest π^*, σ^*, and s conduction bands ($E_f < 10$ eV) at the high-symmetry points of the Brillouin zone.

Point	Band	Willis *et al.* (Ref. 17)	Tatar and Rabii (Ref. 16)	Holzwarth *et al.* (Ref. 18) Slater	Holzwarth *et al.* (Ref. 18) Hedin-Lundqvist
Γ	σ	−20.8	−19.2	−21.5	−20.8
	σ	−20.2	−18.9	−21.3	−20.5
	π	−8.2	−7.9	−8.7	−9.1
	π	−6.7	−6.3	−7.1	−7.0
	σ	−4.7	−4.1	−4.0	−3.2
	σ^*	7.0	7.1	5.5	3.7
	σ^*	7.3	7.3	8.7	9.0
	σ^*	7.7	7.3	8.9	9.3
A	σ		−19.1	−21.4	−20.7
	π		−7.1	−7.9	−8.1
	σ		−4.1	−4.0	−3.2
	s		9.1	8.1	6.5
	σ^*		7.3	8.4	8.9
M	σ	−15.7	−14.6	−16.1	−15.1
	σ	−14.5	−12.2	−14.7	−14.1
	σ	−8.3	−7.2	−7.7	−6.9
	π	−2.7	−2.5	−4.0	−3.1
	π	−2.1	−1.9	−2.7	−2.3
	π^*	1.7	1.7	1.8	1.5
	π^*	2.3	2.2	2.6	2.4
	σ^*	7.2	7.4	6.3	6.7
	σ^*	7.5	7.5	6.8	7.4
L	σ		−14.6		
	σ		−12.2		
	σ		−7.2		
	π		−2.2		
	π^*		1.9		
	σ^*		7.3		

B. Conduction band

If the features of the valence bands are well understood theoretically, this is not the case for the conduction bands. In a simple scheme we have, when going to higher energies, the bottom of the π^*-antibonding band near the P direction, the bottom of a group of σ^* bands at Γ, and the top of the π^* band also at Γ. At higher energy there are many other bands. If the character σ^* and π^* is clear in the ΓMK plane this is not the case for the ALH plane, where the bands are hybridized.[16,18] The important fact of this low-energy conduction-band group is the existence of an almost free-electron-like band with a strong dispersion along the c direction. However, there are strong discrepancies among the calculated positions of these bands.[16,18,19]

Fauster *et al.*[19] have found by inverse photoemission an energy level at the Γ point for $E_f = 4.0 \pm 0.5$ eV. This level has a strong dispersion along Δ and is in agreement with the calculations of Posternak *et al.*[20] This level is not observable by photoemission, because it belongs to the conduction band at an energy lower than the vacuum level. At the Γ point, we found a level at $E_f = 7.6 \pm 0.1$ eV, which presents a very low dispersion in the $U\Delta$ plane, but which is observed only near the line Δ in the $P\Delta$ plane. This is in good agreement with the position of one of the σ^* bands calculated by Tatar and Rabii.[16] We also observed band-structure features around $E_f = 15$ eV along Δ and $E_f = 14$, 16, 21 eV near P. These features are in agreement with the calculations of Tatar and Rabii shifted towards higher energy by 1 eV (Fig. 9). The calculations disagree widely for the position of the three lowest σ^* bands. However, the present study and the one by Fauster *et al.* now provide precise information about two of them.

V. CONCLUSIONS

The ability of varying the photon energy provided by synchrotron radiation, added to the use of a single crystal, allows a very accurate determination of both in-plane and

out-of-plane band structure. Moreover, the spurious effects of the final-state features may be overcome in the determination of the valence bands.

In particular, we described three-dimensional dispersion of the valence bands. The overall shape and positions agree with the published calculations of the band structure.

On the contrary, the conduction bands are not very well described by these models. The strong feature observed recently by inverse photoemission and the results of the present study provide for the first time a set of final-state positions which allows the elaboration of realistic calculations of the conduction band.

ACKNOWLEDGMENTS

The authors are grateful to the staff of the LURE for their support during the experiment. Thanks are due to Dr. H. J. Schubnel (Museum National d'Histoire Naturelle—Paris) for supplying samples of natural graphite single crystals.

[1]G. S. Painter and D. E. Ellis, Phys. Rev. B **1**, 4747 (1970).
[2]D. E. Soule, J. W. McClure, and L. B. Smith, Phys. Rev. **134**, A453 (1964).
[3]J. W. McClure, Phys. Rev. **108**, 612 (1957); **119**, 606 (1960).
[4]R. Chen, P. Trucano, and R. F. Stewart, Acta Crystallogr. Sect. A **33**, 823 (1977).
[5]G. Loupias, J. Chomilier, and D. Guerard, J. Phys. (Paris) Lett. **45**, 6301 (1984).
[6]P. M. Williams, D. Latham, and J. Wood, J. Electron Spectrosc. Related Phenom. **7**, 281 (1975).
[7]A. Bianconi, S. B. M. Hagstrom, and R. Z. Bachrach Phys. Rev. B **16**, 5543 (1977).
[8]W. Eberhardt, I. T. McGovern, E. W. Plummer, and J. E. Fischer, Phys. Rev. Lett. **44**, 200 (1980).
[9]M. Ramm, Deutsche Elektronen-Synchrotron (Hamburg) Interner Bericht No. DESY-F41-HASYLAB-81/04 1981 (unpublished).
[10]A. R. Law, J. J. Barry, and H. P. Hughes, Phys. Rev. B **28**, 5332 (1983).
[11]B. Feuerbacher, B. Fitton, and R. F. Willis, *Photoemission and the Electronic Properties of Surfaces* (Wiley, New York, 1978).
[12]F. Houzay thèse, Université de Paris—Sud, 1983 (unpublished).
[13]N. V. Smith, in *Photoemission in Solids,* Vol. 26 of *Topics in Applied Physics,* edited by M. Cardona and L. Ley (Springer, Verlag, 1978), p. 237.
[14]R. O. Dillon, I. L. Spain, and J. W. McClure, J. Phys. Chem. Solids **38**, 635 (1977).
[15]M. Posternak, A. Baldereschi, A. J. Freeman , and E. Wimmer, Phys. Rev. Lett. **52**, 863 (1984).
[16]R. C. Tatar and S. Rabii, Phys. Rev. B **25**, 4126 (1982).
[17]R. F. Willis, B. Fitton, and G. S. Painter, Phys. Rev. B **9**, 1926 (1974).
[18]N. A. W. Holzwarth, S. G. Louie, and S. Rabii, Phys. Rev. B **26**, 5382 (1982).
[19]Th. Fauster, F. J. Himpsel, J. E. Fischer, and E. W. Plummer, Phys. Rev. Lett. **51**, 430 (1983).
[20]M. Posternak, A. Baldereschi, A. J. Freeman, E. Wimmer, and M. Weinert, Phys. Rev. Lett. **50**, 761 (1983).